Nanoscale

ARTICLE

Imaging magnetic structures of artificial quasicrystal magnets using resonant coherent diffraction of circularly polarized X-rays

Received 00th January 20xx,
Accepted 00th January 20xx

DOI: 10.1039/x0xx00000x

www.rsc.org/

Daeho Sung[†a], Cheolho Jung[†a], Byeong-Gwan Cho[†a], Wonhyuk Jo[b], Hee-Sung Han[c], Ki-Suk Lee[c], Vinayak Bhat[d], Barry Farmer[d], L. E. De Long[d], Ki Bong Lee[a], D. J. Keavney*[e], Dong Ryeol Lee*[b] and Changyong Song*[a]

Unraveling nanoscale spin structures has long been an imporant activity addressing various scientific interests, that are also readily adaptable to technological applications. This has invigorated the development of versatile nanoprobes suitable for imaging specimens in native conditions. Here we have demonstrated resonant coherent diffraction of an arificial quasicrystal magnet with circularly polarized X-rays. Nanoscale magnetic structure was revealed from X-ray speckle patterns by comparing with micromagnetic simulatons, as a step toward understanding intricate relations between chemical and spin structures in an aperiodic quasicrystal lattice. Femtosecond X-ray pulses from free electron lasers are expected to immediately extend the current work to nanoscale structure investigations of ultrafast spin dynamics, surpassing the present spatio-temporal resolution.

1. Introduction

Artificial nanostructures imitating magnetic interactions of real material systems have attracted surging interest by providing a route to modelling and manipulating complex interaction schemes[1]. Frustrated spin configurations in artificially designed nanostructures, for instance, provide a rich platform to induce exotic ground states such as spin ice and composite magnetic monopoles in controlled environments[2-5]. Aperiodic magnetic quasicrystals reproduced by nano-patterned magnets is a system of particular interest[6]. Magnetic ground states are typically understood presuming periodic crystal structures with a translational symmetry, which has been regarded as essential to incorporating long-range magnetic interactions. As such, the discovery of magnetic quasicrystals has attracted attention, and can be expected to expand our understanding of the interrelation between atomic structures of quasicrystals and their magnetic ordering[7-9]. Determining the spatial arrangements of localized ionic spins in magnetic quasicrystals has been hampered by challenges in atomic-scale imaging of three-dimensional spin structures. Artificial quasicrystal magnets therefore become an amenable system to address those issues due to their enlarged spatial scale with magnetic textures that can be readily imaged.

Various microscopic probes are available for imaging magnetic structures at the nanoscale, including Lorentz transmission electron microscopy (TEM), X-ray microscopy, photoemission electron microscopy (PEEM), magnetic force microscopy (MFM), scanning electron microscopy with polarization analysis (SEMPA), etc [10, 11]. Domain imaging of Penrose tiled nanomagnets has been demonstrated for MFM, SEMPA and spin polarized PEEM[12, 13]. As each probe has its own strengths and limitations, probing nanoscale structures via different modalities is important. Sensitivity of the out of plane magnetization component is attained for MFM by probing

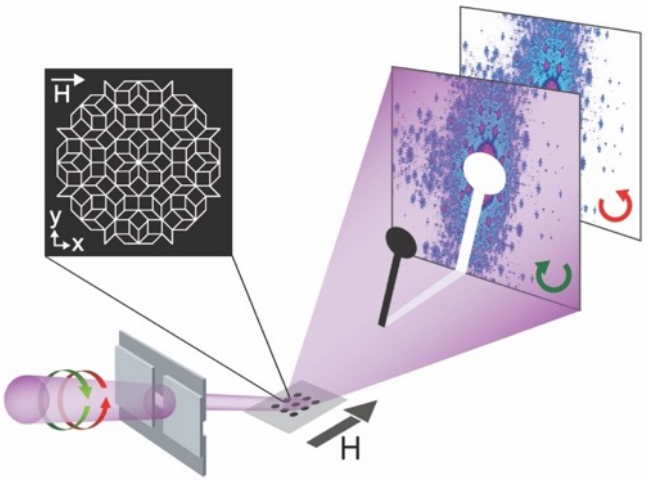

Fig. 1 The schematic of resonant coherent X-ray diffraction in a reflection geometry. Resonant X-ray diffraction experiments were carried out by tuning the incident photon energy at the Fe L3 absorption edge. Circularly polarized coherent X-rays were employed to investigate magnetic structures. X-ray sensitivity on the in-plane spin components is attained. Exit slits define the X-ray beam size.

[a] Department of Physics, POSTECH, Pohang 37673, Korea
[b] Department of Physics, Soongsil University, Seoul 06978, Korea
[c] School of Materials Science and Engineering, Ulsan National Institute of Science and Technology (UNIST), Ulsan 44919, Korea
[d] Department of Physics and Astronomy, University of Kentucky, Lexington, Kentucky 40506, USA
[e] X-ray Science Division, Argonne National Laboratory, Argonne, IL 60439, USA
† Equally contributed to this work.
* Correspondence should be addressed to DJK (keavney@aps.anl.gov), DRL (drlee@ssu.ac.kr) and CYS (cysong@postech.ac.kr).
Electronic Supplementary Information (ESI) available: [details of any supplementary information available should be included here]. See DOI: 10.1039/x0xx00000x

magnetic stray field, which is not effective for the in-plane components. The MFM technique allows the sample to be measured in relatively amenable conditions of temperature, external field at ambient vacuum levels. One of important applications well demonstrating the strength of this MFM includes imaging a magnetic vortex core of permalloy nanodisc[14]. Nanoscale spin textures can be investigated with SEMPA at a few tens of nm resolution, but the probe is surface sensitive. Simultaneous imaging of both ferroelectric and magnetic domains by analyzing backscattered and secondary electrons shows the strength of SEMPA as a multiplex domain imaging probe[15]. PEEM offers strong elemental as well as magnetic contrast, which has been utilized to investigate the dynamic magnetization process by observing the vortex core dynamics[16]. However, the technique is also limited to probing surface layers with relatively short escape lengths of secondary electrons. X-ray microscopy via X-ray optics can be robust, but the imaging with X-ray lens itself introduces different challenges to limit resolution, deteriorate image contrast, etc[11, 17].

Coherent X-rays have enabled lensless imaging of nanoscale object, as demonstrated through coherent diffraction imaging (CDI) and holography, and allow for expanded adaptability by removing ad hoc restriction from imaging optics[18-24]. Element-specific resonant coherent diffraction imaging has been demonstrated to enhance coherent diffraction imaging modality with chemical selectivity[25]. Coherent diffraction imaging via scanning of the sample area with a spatially confined X-ray beam, called ptychography, has spawned a wealth of applications to wide ranged scientific systems of interest, including magnetic systems[26-29]. X-ray sensitivity to magnetic moments is attained from a dichroic effect using circularly polarized X-rays[30, 31]. Despite the remarkable progress, most coherent X-ray imaging of magnetic structures has been focused on specimens mounted on thin membranes to facilitate X-ray transmission, which is not the most generic configuration for most magnetic specimens.

There are also limitations to the measurement of magnetic structure in the transmission geometry. X-ray magnetic circular dichroism (XMCD) is effective only for the spin components parallel to the X-ray beam. This has deterred probing in-plane magnetization in a transmission geometry, unless the sample is tilted at a large angle. Instead measurements in reflection can help to avoid such restrictions. Several results using diffraction microscopies in a reflection geometry have been reported, but imaging magnetic structure has remained challenging [18–20]. Here, by employing a specular reflection of X-rays from a substrate, we report on the application of coherent X-rays to acquire magnetic speckle patterns from artificial quasicrystal magnets patterned on thick non-magnetic substrates. Collected speckle patterns were directly compared with micromagnetic simulations to unveil ground-state magnetic structure of patterned quasicrystal magnets. This work suggests a new route to *in situ* and *in operando* imaging of domain structure of nano-magnets.

2. Experimental

Arrays of artificial quasicrystal magnets of Ammann-Beenker tiling were patterned with permalloy on a non-magnetic Si substrate. The Ammann-Beenker pattern is tiled with square and rhombus structures. Each segment of the permalloy is a single domain nanomagnet having a width of 130 nm, a length of 1,000 nm and the thickness of 25 nm. This nanoscale physical size of each segment is carefully chosen to accommodate a single ferromagnetic domain while avoiding unwanted super-paramagnet feature accompanied in a smaller scale. This single-domain nanomagnet segment is the key to successfully imitate aperiodic magnetic quasicrystals through the artificial pattern. The sample image (in Fig. 1) shows one

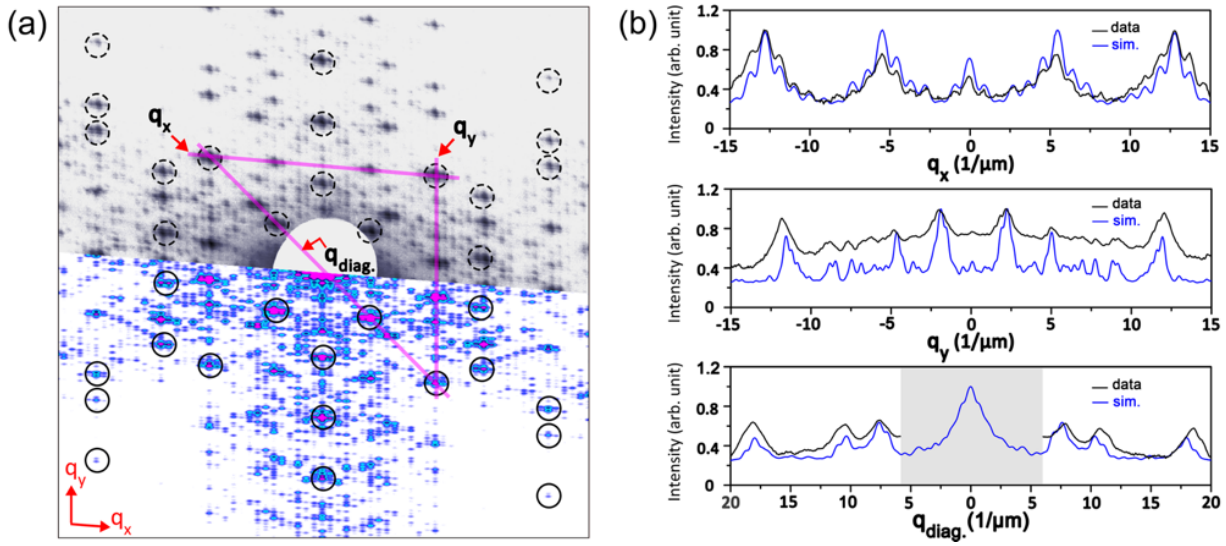

Fig. 2 An X-ray speckle pattern from an artificial quasicrystal magnet array. (a) Measured speckle pattern is displayed in gray (upper panel) and calculated speckle pattern is shown in color for comparison (lower panel). The white semicircle in the middle of the measured data is the region blocked by the beam stopper (see text). Expected peak positions are marked with broken black circles overlayed with the measured speckle pattern in the upper panel showing excellent agreement between the calculations and experiments. (b) For a quantitative analysis, line plots were compared showing agreements in peak positions and intensities. Lines were cut along major axis of qx, qy, and the diagonal direction shown with the purple lines in (a).

Ammann-Beenker tiled quasicrystal magnet. The dark region in the inset is Si substrates and the bright areas are permalloy segments. A detailed description of the sample is provided elsewhere[32].

Coherent X-ray speckle patterns were measured at the 4-ID-C undulator beamline of the Advanced Photon Source. Incident X-ray energy was tuned to the Fe L_3 absorption edge to attain signal enhancements from Fe magnetic moments. Right and left circularly polarized (RCP & LCP) X-rays were made using a circularly polarized undulator. The coherent X-ray diffraction experiment was performed in a reflection geometry with the y-axis perpendicular to the scattering plane as shown in Fig. 1. The size of incident X-ray beam was defined using 50-micron slits for both horizontal and vertical directions.

Diffraction patterns were collected in a specular reflection configuration with the incident angle of X-rays at 22.5 degree. The size of X-ray footprint on the sample is 130 μm by 50 μm along the sample x- and y-direction, respectively. The X-ray beam size is chosen as a favourable condition for experiments, for instance maintaining decent amount of photon flux by not significantly deteriorating the degree of spatial coherence. The resolution of the sample image, determined from the highest detectable diffraction angle, is independent of the X-ray beam size in this coherent diffraction imaging technique[21]. The sample is mounted inside a UHV chamber in which a magnetic field can be applied. This artificial quasicrystal magnet has the magnetic anisotropy with in-plane easy axes. Coherent X-ray diffraction experiments were carried out for the specimen at remanent condition after turning off the external field applied along the in-plane x-direction of 5000 Oe, which is above the saturation field of 1000 Oe. The scattering plane is defined in the xz-plane. Resonant coherent X-ray diffraction patterns were measured using a charge coupled device (CCD) detector installed at 1.05 m downstream of the sample. A beam-stopper was placed in

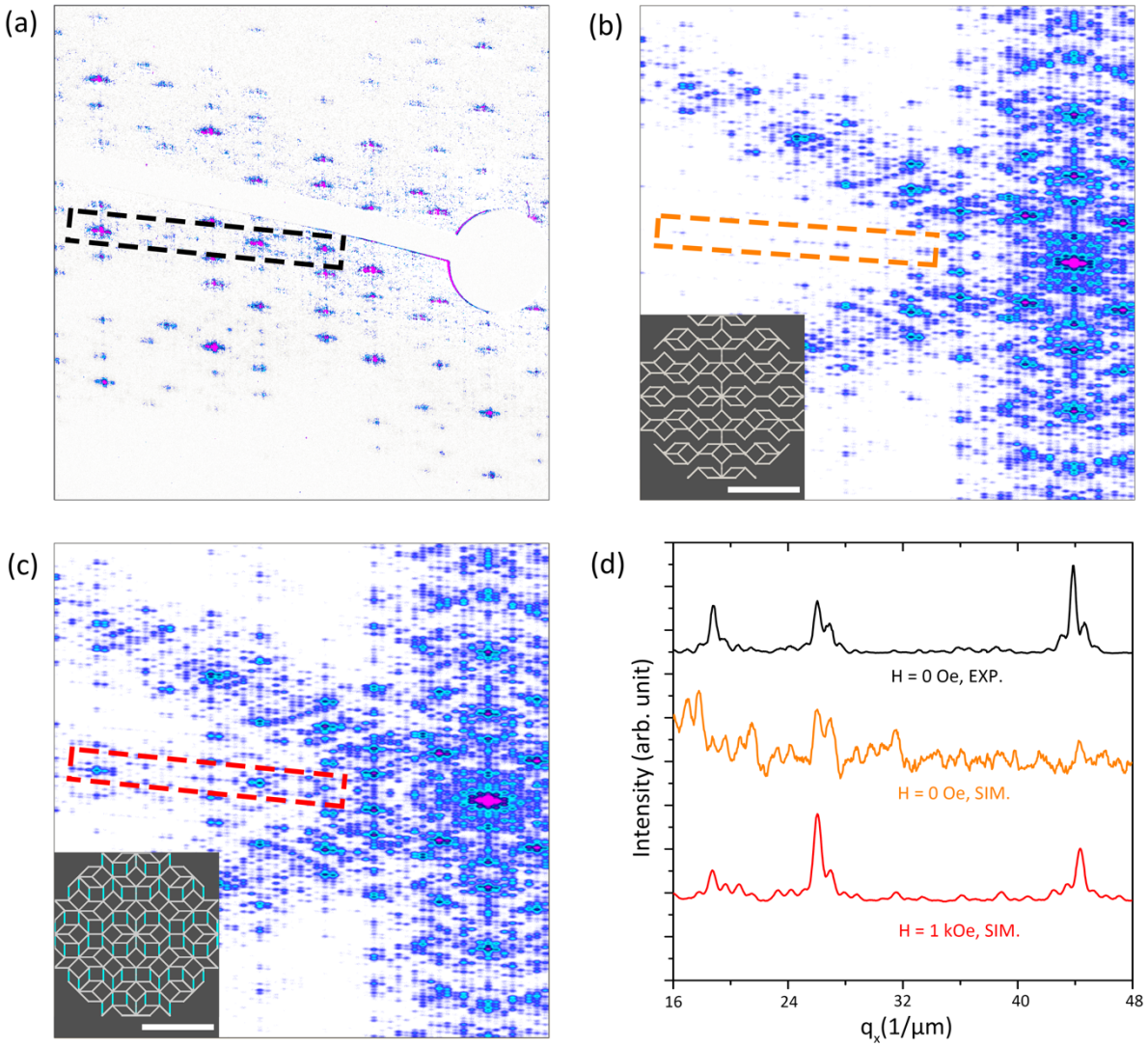

Fig. 3 Comparison of the magnetic speckle patterns from resonant coherent diffractions of circularly polarized X-rays and simulations. (a) Measured magnetic speckle patterns obtained by subtracting two speckle patterns of RCP and LCP X-rays for the sample in a remanent state. (b) Calculated magnetic speckle pattern for the anticipated magnetic structure of the remanent state expected from micromagnetic simulations. (c) Calculated magnetic speckle pattern for the saturated state. Insets in (b & c) show the x-component of the spin structures obtained from micromagnetic simulations, upon which the speckle patterns were calculated. Cyan-color segments in the inset are vertical components missed in the remanent state. (d) Line plots cut from the region marked with the rectangular boxes of the speckle patterns in (a-c). Scale bars shown in the artificial magnet array in (b) and (c) is 5 μm.

front of the CCD to block the direct X-ray beam reflected from the sample surface. Speckle patterns revealing the magnetic structure were obtained by comparing patterns from LCP and RCP X-rays.

3. Results and discussion

Recorded speckle patterns were analysed by comparing with the calculated coherent speckle patterns of the sample. The speckle pattern obtained by averaging the two coherent diffraction patterns of RCP and LCP X-rays reflects on the charge distribution of the specimen, shown with a gray colour in the upper panel of Fig. 2(a). The white semicircle area at the center is the part of speckle pattern blocked by the beam-stopper. The measured speckle pattern was then compared directly with the calculated pattern of the patterned quasicrystal magnet sample shown in Fig. 1 by taking into account of the X-ray illumination area, detector pixel size, X-ray wavelength, and the sample-to-detector distance of 1.05 m[11,22,23]. The small slanting of the qx axis from a perpendicular line of qy is due to a slight tilting of the CCD detector along y & z coordinates, which is also considered in the simulation in the lower panel of Fig. 2(a). Main features such as strong peak positions of the coherent speckle patterns were compared. Intense diffraction peaks marked with circles are in good agreement with the measured pattern supporting the validity of the simulation.

The comparison was extended using line plots shown in Fig. 2(b). Line plots were cut through the major axis of qx, qy, and $\sqrt{qx^2 + qy^2}$ of diagonal direction (q_{diag}). Compared to the simulation, measured diffraction peaks appear at low contrast, which is attributed to the insufficient spatial degree of coherence in the incident X-rays and low signal-to-noise ratio. Overall, however, excellent agreement of the calculated pattern with the measured one was achieved, which vindicates the quality of the simulation and experiment in Fig. 2. Obtained high accuracy of the simulation further confirms that nanoscale image of the specimen can be successfully interpreted by comparing with the simulated pattern.

Next, we turn to the spin structure of the artificial quasicrystal magnet. The sensitivity of coherent X-ray diffraction signals to magnetic structures is gained from the magnetic circular dichroic (MCD) effect with the direction selective sensitivity of magnetization to the direction of the helicity of incident X-rays. The reflection geometry that we have used for this resonant coherent X-ray diffraction imaging experiment is crucial for imaging spin structure of this patterned quasicrystal magnet. It enables us to gain an MCD sensitivity to the magnetic structure of the sample having an in-plane magnetic anisotropy, which cannot be detected in the transmission geometry. Figure 3 compares the measured magnetic speckle pattern ($I_{RCP}(q) - I_{LCP}(q)$) with calculations made for magnetic structures at remanent and saturation condition. Whilst the measured magnetic speckle pattern in Fig. 3(a) appears in low contrast with low signal-to-noise ratio (SNR), strong diffraction peaks are clearly identified, which provides sufficient experimental evidence to identify spin structures.

To unravel the spin structure, the measured magnetic speckle pattern was compared with a calculated one in Fig. 3(b), which reflects on the remanent state spin structure obtained from micromagnetic simulations using the mumax[3] code[33]. The micromagnetic simulation is a common and well-proven method of calculating the static and dynamic behaviors of nanomagnetism supporting the pertinence in simulating the current artificial quasicrystal magnet made of nanoscale segments[34]. Model system in micromagnetic simulations was the Ammann-Beenker pattern with the same spatial dimensions and parameters used in the experiments. The typical parameters of permalloy were used: saturation magnetization M_s = 860 kA/m; exchange stiffness A_{ex} = 13 pJ/m; and zero magnetocrystalline anisotropy and the pixel size of 10 × 10 × 25 nm^3. The real space image of the spin structure of this remanent state from the micromagnetic simulations is shown as an inset in Fig. 3(b) and ESI. Except for the lower contrast in the measured data of Fig. 3(a), overall features are well reproduced in the simulation. However, the strong diffraction peaks along the equator (qy) line apparent in Fig.3(a) are missing in the simulation in Fig. 3(b). The rectangular broken boxes in Fig. 3(a) and Fig. 3(b) emphasize the difference, implying that the remanent state spin structure from micromagnetic simulation has missed some structural details.

A new simulation was then performed for a different spin structure to improve the calculated spin structure. The calculated magnetic speckle pattern for the spin structure under a saturation field is shown in Fig. 3(c). The inset in Fig. 3(c) shows the x-component of the spin structure at saturation obtained from the micromagnetic simulations, for which the magnetic speckle pattern is calculated. The missed diffraction peaks in Fig. 3(b) along the equator (qy) is better recovered now in Fig. 3(c), which shows much improved agreement with the experimental results in Fig. 3(a). More quantitative comparisons were made with line plots in Fig. 3(d). Line plots in Fig. 3(d) display diffraction peaks in the boxed regions of Fig. 3(a-c). The line plots clearly exhibit that the simulation with spin configuration at saturation better matches the experimental data.

One notes that the main difference between the two spin structures of Fig. 3(b) and Fig. 3(c) lies in the existence of the x-component of magnetization in the vertical (y-direction) segments (colored in cyan in Fig. 3(c)) of the artificial quasicrystal magnet. The zero-field spin structure in the inset of Fig. 3(b) contains no magnetization in the vertical segments. In contrast, the vertical segment of the spin structure at saturation has non-vanishing x-directional magnetization, coloured in red for emphasis in Fig. 3(c). The presence of x-component magnetization in the vertical segment of the artificial quasicrystal magnet accounts for presence of strong diffraction peaks along the equator in experiment. Observation of remained x-component magnetization in the vertical segments at remanent state may be attributed to a small slanting of the sample axis with the external field direction, different from the micromagnetics simulations. This comparison study thereby yields a more precise nanoscale spin structure of the artificial

quasiperiodic magnet obtained from resonant coherent X-ray diffraction patterns.

4. Conclusions

The magnetic structure of Ammann-tiled artificial quasicrystal magnet arrays on a thick Si substrate is obtained from resonant coherent diffraction with circularly polarized X-rays at the Fe L_3 absorption edge. We have demonstrated a successful application of resonant coherent X-ray diffraction in specular reflection for investigating in-plane nanoscale spin structure. The spin structure of the artificial quasicrystal magnet was extracted by directly comparing the measured speckle patterns with micromagnetic simulations. It provides a reliable approach to obtaining real space image from speckle patterns with relatively low SNR, insufficient spatial coherence, etc. This resonant coherent X-ray diffraction investigation of a functional nano-magnet bears a particular significance with the potential to ultrafast nanoscale imaging by employing femtosecond X-ray laser pulses from X-ray free electron lasers (XFELs)[35]. The femtosecond X-ray laser pulses from XFELs can overcome the radiation-damage limited resolution barriers by acquiring the diffraction signals prior to the onset of radiation damages[36-40]. It will greatly expand our understanding on nanoscale phenomena at femtosecond temporal scale.

Conflicts of interest

There are no conflicts to declare.

Author contribution

DL, DK & CS conceived the projects. DS, CJ & CS analyzed the data by simulating the speckle patterns. HH & KL performed micromagnetics simulations. VB, BF & LL provided the samples. All authors are involved in the experiments. DS and CS wrote the manuscript with inputs from all authors.

Acknowledgements

This work was supported by National Research Foundation of Korea (Grant No. NRF-2015R1A15A1009962, NRF-2016R1A2B3010980, NRF-2017K1A3A7A09016380 & NRF-2016K1A3A7A09005585). This research used resources of the Advanced Photon Source, a U.S. Department of Energy (DOE) Office of Science User Facility operated for the DOE Office of Science by Argonne National Laboratory under Contract No. DE-AC02-06CH11357. Research at the University of Kentucky was supported by U.S. Department of Energy (Grant No. DE-SC0016519. We thank B.-D. Lee and J.-W. Kim at the APS for their helpful comments and discussions.

Notes and References

1. J. P. Morgan, A. Stein, S. Langridge and C. H. Marrows, *Nature Physics*, 2010, **7**, 75.
2. J. Trastoy, M. Malnou, C. Ulysse, R. Bernard, N. Bergeal, G. Faini, J. Lesueur, J. Briatico and J. E. Villegas, *Nature Nanotechnology*, 2014, **9**, 710.
3. C. Castelnovo, R. Moessner and S. L. Sondhi, *Nature*, 2008, **451**, 42.
4. R. F. Wang, C. Nisoli, R. S. Freitas, J. Li, W. McConville, B. J. Cooley, M. S. Lund, N. Samarth, C. Leighton, V. H. Crespi and P. Schiffer, *Nature*, 2006, **439**, 303.
5. S. Ladak, D. E. Read, G. K. Perkins, L. F. Cohen and W. R. Branford, *Nature Physics*, 2010, **6**, 359.
6. D. Shi, Z. Budrikis, A. Stein, S. A. Morley, P. D. Olmsted, G. Burnell and C. H. Marrows, *Nature Physics*, 2017, DOI: 10.1038/s41567-017-0009-4.
7. A. I. Goldman, T. Kong, A. Kreyssig, A. Jesche, M. Ramazanoglu, K. W. Dennis, S. L. Bud'ko and P. C. Canfield, *Nature Materials*, 2013, **12**, 714.
8. K. Deguchi, S. Matsukawa, N. K. Sato, T. Hattori, K. Ishida, H. Takakura and T. Ishimasa, *Nature Materials*, 2012, **11**, 1013.
9. A. I. Goldman, *Science and Technology of Advanced Materials*, 2014, **15**, 044801.
10. M. R. Scheinfein, J. Unguris, M. H. Kelley, D. T. Pierce and R. J. Celotta, *Review of Scientific Instruments*, 1990, **61**, 2501-2527.
11. F. Peter, *Journal of Physics D: Applied Physics*, 2017, **50**, 313002.
12. V. S. Bhat, J. Sklenar, B. Farmer, J. Woods, J. T. Hastings, S. J. Lee, J. B. Ketterson and L. E. De Long, *Physical Review Letters*, 2013, **111**, 077201.
13. B. Farmer, V. S. Bhat, A. Balk, E. Teipel, N. Smith, J. Unguris, D. J. Keavney, J. T. Hastings and L. E. De Long, *Physical Review B*, 2016, **93**, 134428.
14. T. Shinjo, T. Okuno, R. Hassdorf, K. Shigeto and T. Ono, *Science*, 2000, **289**, 930.
15. J. Unguris, S. R. Bowden, D. T. Pierce, M. Trassin, R. Ramesh, S. W. Cheong, S. Fackler and I. Takeuchi, *APL Materials*, 2014, **2**, 076109.
16. S. B. Choe, Y. Acremann, A. Scholl, A. Bauer, A. Doran, J. Stöhr and H. A. Padmore, *Science*, 2004, **304**, 420.
17. S. Woo, K. Litzius, B. Krüger, M.-Y. Im, L. Caretta, K. Richter, M. Mann, A. Krone, R. M. Reeve, M. Weigand, P. Agrawal, I. Lemesh, M.-A. Mawass, P. Fischer, M. Kläui and G. S. D. Beach, *Nature Materials*, 2016, **15**, 501.
18. J. Miao, T. Ishikawa, I. K. Robinson and M. M. Murnane, *Science*, 2015, **348**, 530.
19. I. Robinson and R. Harder, *Nature Materials*, 2009, **8**, 291.
20. S. Eisebitt, J. Lüning, W. F. Schlotter, M. Lörgen, O. Hellwig, W. Eberhardt and J. Stöhr, *Nature*, 2004, **432**, 885.
21. H. N. Chapman and K. A. Nugent, *Nature Photonics*, 2010, **4**, 833.
22. D. Nam, J. Park, M. Gallagher-Jones, S. Kim, S. Kim, Y. Kohmura, H. Naitow, N. Kunishima, T. Yoshida, T. Ishikawa and C. Song, *Physical Review Letters*, 2013, **110**, 098103.
23. X. Huang, J. Nelson, J. Kirz, E. Lima, S. Marchesini, H. Miao, A. M. Neiman, D. Shapiro, J. Steinbrener, A. Stewart, J. J. Turner and C. Jacobsen, *Physical Review Letters*, 2009, **103**, 198101.
24. J. A. Rodriguez, R. Xu, C.-C. Chen, Z. Huang, H. Jiang, A. L. Chen, K. S. Raines, A. Pryor Jr, D. Nam, L. Wiegart, C. Song,

A. Madsen, Y. Chushkin, F. Zontone, P. J. Bradley and J. Miao, *IUCrJ*, 2015, **2**, 575-583.
25. C. Song, R. Bergstrom, D. Ramunno-Johnson, H. Jiang, D. Paterson, M. D. de Jonge, I. McNulty, J. Lee, K. L. Wang and J. Miao, *Physical Review Letters*, 2008, **100**, 025504.
26. M. D. Seaberg, B. Zhang, D. F. Gardner, E. R. Shanblatt, M. M. Murnane, H. C. Kapteyn and D. E. Adams, *Optica*, 2014, **1**, 39-44.
27. F. Pfeiffer, *Nature Photonics*, 2018, **12**, 9-17.
28. C. Phatak, Y. Liu, E. B. Gulsoy, D. Schmidt, E. Franke-Schubert and A. Petford-Long, *Nano Letters*, 2014, **14**, 759-764.
29. A. Tripathi, J. Mohanty, S. H. Dietze, O. G. Shpyrko, E. Shipton, E. E. Fullerton, S. S. Kim and I. McNulty, *Proceedings of the National Academy of Sciences*, 2011, **108**, 13393.
30. G. van der Laan, B. T. Thole, G. A. Sawatzky, J. B. Goedkoop, J. C. Fuggle, J.-M. Esteva, R. Karnatak, J. P. Remeika and H. A. Dabkowska, *Physical Review B*, 1986, **34**, 6529-6531.
31. P. Carra and M. Altarelli, *Physical Review Letters*, 1990, **64**, 1286-1288.
32. V. S. Bhat, J. Sklenar, B. Farmer, J. Woods, J. B. Ketterson, J. T. Hastings and L. E. De Long, *Journal of Applied Physics*, 2014, **115**, 17C502.
33. D. Kumar and A. O. Adeyeye, *Journal of Physics D: Applied Physics*, 2017, **50**, 343001.
34. A. Fernández-Pacheco, R. Streubel, O. Fruchart, R. Hertel, P. Fischer and R. P. Cowburn, *Nature Communications*, 2017, **8**, 15756.
35. J. Miao, R. L. Sandberg and C. Song, *IEEE Journal of Selected Topics in Quantum Electronics*, 2012, **18**, 399-410.
36. M. Gallagher-Jones, Y. Bessho, S. Kim, J. Park, S. Kim, D. Nam, C. Kim, Y. Kim, D. Y. Noh, O. Miyashita, F. Tama, Y. Joti, T. Kameshima, T. Hatsui, K. Tono, Y. Kohmura, M. Yabashi, S. S. Hasnain, T. Ishikawa and C. Song, *Nature Communications*, 2014, **5**, 3798.
37. H. N. Chapman, C. Caleman and N. Timneanu, *Philosophical Transactions of the Royal Society B: Biological Sciences*, 2014, **369**.
38. T. Kimura, Y. Joti, A. Shibuya, C. Song, S. Kim, K. Tono, M. Yabashi, M. Tamakoshi, T. Moriya, T. Oshima, T. Ishikawa, Y. Bessho and Y. Nishino, *Nature Communications*, 2014, **5**, 3052.
39. C. Song, K. Tono, J. Park, T. Ebisu, S. Kim, H. Shimada, S. Kim, M. Gallagher-Jones, D. Nam, T. Sato, T. Togashi, K. Ogawa, Y. Joti, T. Kameshima, S. Ono, T. Hatsui, S. Iwata, M. Yabashi and T. Ishikawa, *Journal of Applied Crystallography*, 2014, **47**, 188-197.
40. R. Xu, H. Jiang, C. Song, J. A. Rodriguez, Z. Huang, C.-C. Chen, D. Nam, J. Park, M. Gallagher-Jones, S. Kim, S. Kim, A. Suzuki, Y. Takayama, T. Oroguchi, Y. Takahashi, J. Fan, Y. Zou, T. Hatsui, Y. Inubushi, T. Kameshima, K. Yonekura, K. Tono, T. Togashi, T. Sato, M. Yamamoto, M. Nakasako, M. Yabashi, T. Ishikawa and J. Miao, *Nature Communications*, 2014, **5**, 4061.

